ORIGINAL ARTICLE

Upscaling semi-adiabatic measurements for simulating temperature evolution of mass concrete structures

Wilson Ricardo Leal da Silva · Vít Šmilauer · Petr Štemberk

Abstract Thermal analysis of mass concrete is often carried out through finite element (FE) analysis. The heat release rate in a material point can be determined from a small-scale isothermal calorimeter. Nonetheless, isothermal calorimeter is generally an expensive device and lacks practicality. In that light, this paper proposes a low-cost semi-adiabatic calorimeter setup complemented with a FE analysis. Such a combination provides evolution of hydration heat under isothermal temperature and enables upscaling to the temperature evolution in mass concrete structures. The upscaling process is demonstrated on three mass concrete blocks. Initially, semi-adiabatic measurements start on 14 dm^3 concrete cube to identify the heat release rate. Next, the calibrated hydration model is upscaled and validated on a 1.0 m^3 concrete cube and two mass concrete foundation blocks with 511 and 1,050 m^3. The validation proves successfully the upscaling approach; also, the same temperature-dependent hydration kinetics performs well from small to large scales.

Keywords Cement hydration · Mass concrete · Upscaling · Temperature · Semi-adiabatic experiment

1 Introduction

The term "mass concrete" describes concrete members where high thermal gradients may lead to cracking. Binder content and initial concrete temperature belong to the most critical factors; even concrete members that are only 0.5 m in thickness may be susceptible to thermal cracking [23]. Temperature gradients emerge as a result of concrete's low thermal conductivity, the exothermic hydration process, and the surrounding ambient temperature. Consequently, significant tensile stresses may develop, leading to early age thermal cracking and thus compromising concrete durability [29].

Several protective measures to avoid concrete cracking were developed and a comprehensive list and practical guidelines for mass concrete were formulated [1, 21, 23]. For example, the cooling rate should not exceed 3 °C/h during the first 24 h and caution is necessary in cold weather when concrete temperature falls below 4 °C [22, 24]. Furthermore,

W. R. L. da Silva (✉) · V. Šmilauer
Department of Mechanics, Faculty of Civil Engineering, Czech Technical University in Prague, Thákurova, 7 166 29, Prague 6, Czech Republic
e-mail: wilson.silva@fsv.cvut.cz

V. Šmilauer
e-mail: vit.smilauer@fsv.cvut.cz

P. Štemberk
Department of Concrete and Masonry Structures, Faculty of Civil Engineering, Czech Technical University in Prague, Thákurova, 7 166 29, Prague 6, Czech Republic
e-mail: stemberk@fsv.cvut.cz

studies and experience have shown that surface cracking can be minimized or avoided when the maximum differential temperature between the interior and exterior surface of concrete is limited to less than 20 °C [20]. In addition, the temperature in structural concrete should never exceed 70 °C during hardening in order to avoid the formation of delayed ettringite accompanied by expansion [2].

Several complex thermo-chemo–mechanical models were formulated during the last decades. They include prediction of thermal stresses, concrete creep or early-age cracking [13, 14, 16, 18, 26, 28]. A remarkably high number of input parameters involved render them difficult for daily use. In this regard, this paper focuses on temperature evolution only.

Predicting temperature rise and its gradients present a classical approach for crack mitigation. Hydration models are largely responsible for this task. To mention a few of them, the CEMHYD3D model based on cellular automata [3] or the model based on the theory of reactive porous media [11] are remarkable. Our approach relies on a modified kinetic model for concrete by Cervera et al. [9] in which the hydration is approximated through the chemical affinity as a four-parametric function. The affinity function can be easily calibrated from isothermal calorimetry.

However, semi-adiabatic experimental setup is used more extensively due to its simplicity and availability. As opposed to isothermal calorimetry,

temperature evolution depends now on heat capacity, boundary conditions, and concrete temperature. In order to consider nonhomogeneous temperature across a sample, finite element (FE) simulation is needed. Figure 1 shows such a work flow, accommodating the same hydration model on several length scales. The main objective of this paper focuses on upscaling from semi-adiabatic measurements to mass concrete structures, starting from 14 dm^3 and ending at 1,050 m^3 concrete block.

2 Thermal field analysis and affinity hydration model

2.1 Weak formulation of heat transport

The transient three dimensional heat conduction problem in incompressible media is derived from a well-known energy balance on a differential element. The combination of that with Fourier's law leads to the differential equation

$$\lambda(\mathbf{x})\Delta T(\mathbf{x}) + \overline{Q}(\mathbf{x}, t) = \rho(\mathbf{x})c_V(\mathbf{x})\frac{\partial T(\mathbf{x}, t)}{\partial t}, \qquad (1)$$

where $T(\mathbf{x}, t)$ (K) is the unknown temperature field, $\lambda(\mathbf{x})$ (W m^{-1} K^{-1}) is the thermal conductivity of an isotropic material, $\rho(\mathbf{x})$ (kg/m^3) is the material density, $c_V(\mathbf{x})$ (J kg^{-1} K^{-1}) is the specific heat capacity,
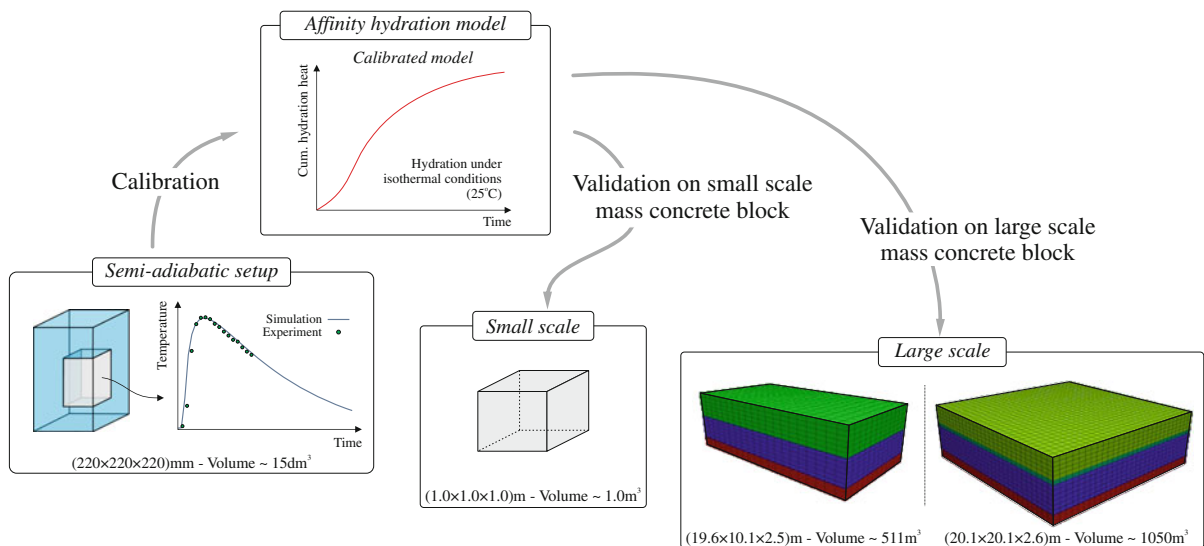

Fig. 1 Upscaling semi-adiabatic temperature measurements: a calibrated hydration model is used for validation on mass concrete blocks

and $\overline{Q}(\mathbf{x}, t)$ (W/m^3) represents a known heat source, in this case, the concrete hydration heat. Initial and boundary conditions can be assigned to Eq. (1).

A weak solution is obtained by multiplying Eq. (1) with a virtual temperature field [27]. After a short elaboration, a weak formulation reads

$$\mathbf{C}\dot{\mathbf{r}} + \mathbf{K}\mathbf{r} = \mathbf{p}, \qquad (2)$$

where $\mathbf{K}$ is the conductivity matrix, $\mathbf{C}$ is the capacity matrix, and $\mathbf{p}$ is the heat load vector, which captures both the boundary conditions and the heat source. Using a matrix of shape functions $\mathbf{N}$ and a matrix for temperature gradient interpolation $\mathbf{B}$, $\mathbf{K}$, $\mathbf{C}$, and $\mathbf{p}$ are presented as follows

$$\mathbf{K} = \int_{\Omega} \mathbf{B}(\mathbf{x})^T \lambda(\mathbf{x}) \mathbf{B}(\mathbf{x}) d\Omega, \qquad (3)$$

$$\mathbf{C} = \int_{\Omega} \mathbf{N}(\mathbf{x})^T \rho(\mathbf{x}) c_{\mathrm{V}}(\mathbf{x}) \mathbf{N}(\mathbf{x}) d\Omega, \qquad (4)$$

$$\mathbf{p} = -\int_{\Gamma_{c,T,\bar{q}}} \mathbf{N}(\mathbf{x})^T \mathbf{n}(\mathbf{x})^T \mathbf{q}(\mathbf{x}, t) \, d\Gamma$$
$$+ \int_{\Omega} \mathbf{N}(\mathbf{x})^T \overline{\mathbf{Q}}(\mathbf{x}, \, t, \, \mathbf{r}) d\Omega. \qquad (5)$$

Temperature-dependent terms will appear directly on the left hand side of Eq. (2). However, the heat source $\overline{Q}(\mathbf{x}, t, \mathbf{r})$ is coupled nonlinearly with temperature and a v-form version of the trapezoidal scheme is used in the form of predictor-corrector scheme. After a few iterations, Eq. (2) satisfies sufficiently both the heat balance on a structure and the temperature-dependent heat source in a material point [17, 27].

2.2 Affinity hydration model

The affinity hydration model provides a framework for accommodating all stages of cement hydration. It considers hydrating cement under isothermal temperature at 25 °C. The rate of hydration can be expressed by the chemical affinity $\widetilde{A}_{25}(DoH)$ as

$$\frac{d\mathrm{DoH}}{dt} = \widetilde{A}_{25}(DoH), \qquad (6)$$

where the chemical affinity has a dimension of 1/time. The affinity for isothermal temperature can be obtained experimentally; in particular, the isothermal

calorimetry measures a heat flow $q(t)$, which gives the hydration heat $Q(t)$ after integration.

Cervera et al. [9] proposed an analytical form of the normalized affinity, which was further refined by Gawin et al. [13]. A slightly modified formulation is proposed in this work

$$\widetilde{A}_{25}(DoH) = B_1 \left(\frac{B_2}{DoH_\infty} + DoH \right)$$
$$\cdot (DoH_\infty - DoH) \exp\left(-\bar{\eta} \frac{DoH}{DoH_\infty} \right), \quad (7)$$

where B_1 and B_2 are coefficients to be adjusted, DoH_∞ is the ultimate hydration degree, and $\bar{\eta}$ represents the micro-diffusion of free water through formed hydrates.

The parameters from Eq. (7), i.e. B_1, B_2, DoH_∞, and $\bar{\eta}$, express isothermal hydration at 25 °C. When hydration proceeds under varying internal temperatures, which normally happens, the affinity $\widetilde{A}_{25}$ is scaled via Arrhenius equation to an arbitrary temperature T (K) by

$$\widetilde{A}_{\mathrm{T}} = \widetilde{A}_{25} \cdot \exp\left[\frac{\mathrm{E_a}}{\mathrm{R}} \cdot \left(\frac{1}{273.15 + 25} - \frac{1}{\mathrm{T}} \right) \right], \qquad (8)$$

where R (J mol^{-1} K^{-1}) is the universal gas constant and E_a (J/mol) is the activation energy.

For example, simulating isothermal hydration at 35 °C means scaling $\widetilde{A}_{25}$ with a factor of 1.651 at a given time. This means that hydrating concrete for 10 h at 35 °C releases the same amount of heat as concrete hydrating for 16.51 h under 25 °C. Notice that setting $E_a = 0$ in Eq. (8) ignores the effect of temperature, i.e. it assumes the hydration under 25 °C.

2.3 Performance of affinity hydration model

The affinity hydration from Eq. (7) performs well on all OPC-derived binders. Table 1 summarizes some of the parameters of the affinity model, whereas Fig. 2 validates them graphically against the isothermal calorimetry data or CEMHYD3D simulation [3]. In all cases presented in Table 1 the DoH_∞ was set at 0.85. Moreover, all results were scaled to isothermal temperature 25 °C by recalculating them with the activation energy of 38.3 kJ/mol. The water/binder ratio was in the range of 0.4–0.5; hence, the hydration is almost uninfluenced by a lack of water for hydration. If not so, the DoH_∞ needs to be reduced.

Table 1 Parameters for affinity hydration model ($DoH_\infty = 0.85$)

Binder name	B_1 (h^{-1})	B_2 (–)	$\bar{\eta}$ (–)	Q_{pot} (J/g)
CEM I 32.5R Mitani[a]	0.5846	1.4e–3	7.0	471
CEM I 42.5R Mokra[b]	1.2667	8.0e–6	7.4	495
CEM I 42.5R Prachovice[b]	0.9744	7.0e–4	6.7	509
CEM I 52.5R Princigallo[b]	1.3641	6.0e–5	5.8	518
CEM II/A-S 42.5 Mokra[a]	0.9744	7.0e–4	6.7	420
CEM II/B-S 32.5R Mokra[a]	0.9744	7.0e–4	6.7	370
CEM III/B 32.5 Mokra[a]	0.5846	5.0e–3	8.0	355

[a] Validation via isothermal calorimetry

[b] Validation via CEMHYD3D hydration model
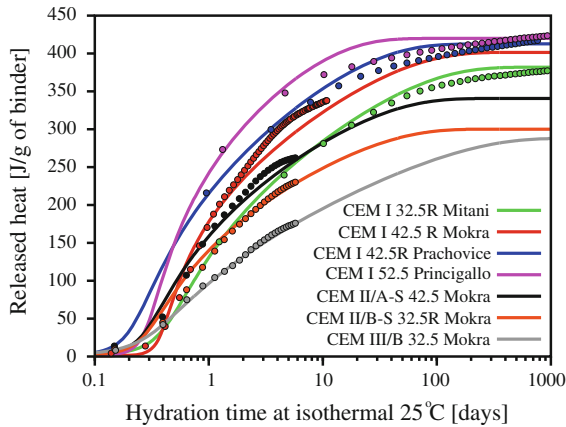
Fig. 2 Validation of affinity hydration model on OPC-based cements

The potential hydration heat (Q_{pot}) is understood as the total released heat of a finely-ground binder after roughly 3 years under saturated conditions. The maximum degree of hydration (DoH_∞) never reaches one due to a presence of large cement grains and unreacted supplementary materials.

3 Calibration on a 14 dm³ concrete specimen

According to Fig. 1, the upscaling starts by calibrating the hydration model. A concrete cube with 240 mm edge surrounded with a 100 mm thick polystyrene foam is used (see Fig. 3). The temperature was recorded by a K-type thermocouple placed in the
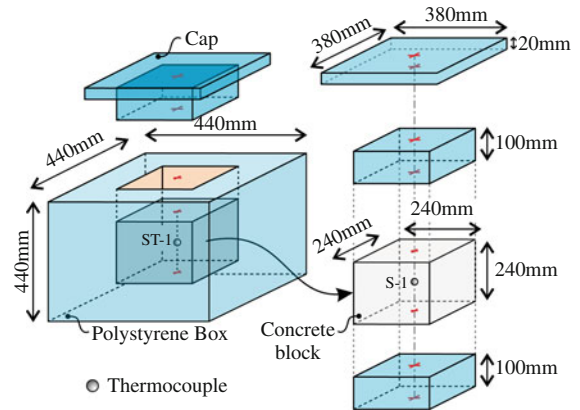

Fig. 3 Proposed experimental setup

Table 2 Composition in kg/m³ for concrete mixtures used in upscaling and validation

Concrete block	14 dm³, 1 m³, 511 m³		1,050 m³		
Concrete designation	C1	C2	C3	C4	C5
Binder CP IV RS	420.0	408.0	345.9	340.9	314.4
River Sand (S)	750.0	720.0	292.4	288.1	300.0
Crushed-stone sand (CS)	–	–	585.6	577.0	600.7
Coarse aggregate 1 (CA1)	1.020	255.0	250.1	246.5	248.3
Coarse aggregate 2 (CA2)	–	765.0	750.3	739.4	744.8
Water	138.6	140.7	128.6	126.7	127.6
Crushed ice	59.4	60.3	55.1	54.3	54.7
Water reducing admixture[a] (%)	0.65	0.65	1.0	1.0	1.0
High range water reducing admixture[a] (%)	0.44	0.32	0.15	0.15	0.40
Retarder agent[a] (%)	–	–	0.30	0.70	–

[a] Percent of binder mass

Table 3 Physical properties of the aggregates

Aggregate	S	CS	CA1	CA2
Max. grain size (mm)	1.18	2.40	12.5	25.0
Fineness modulus (–)	1.41	2.48	5.97	7.07
Dust content (%)	1.1	14.5	1.0	1.1
Specific gravity (–)	2.63	2.84	2.65	2.65

Fig. 5 Small scale mass concrete block 1.0 m³: geometry, temperature gauges, discretization, boundary conditions and temperature field at 15.5 h
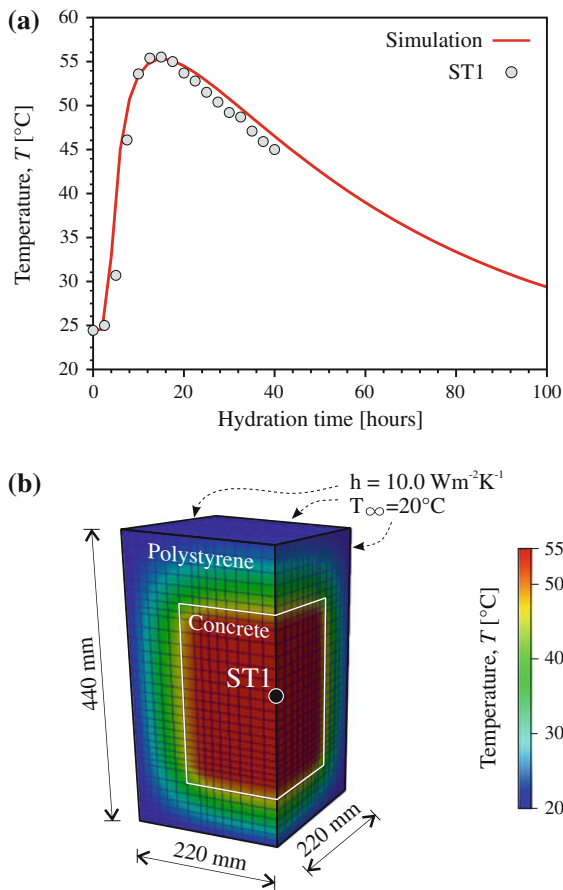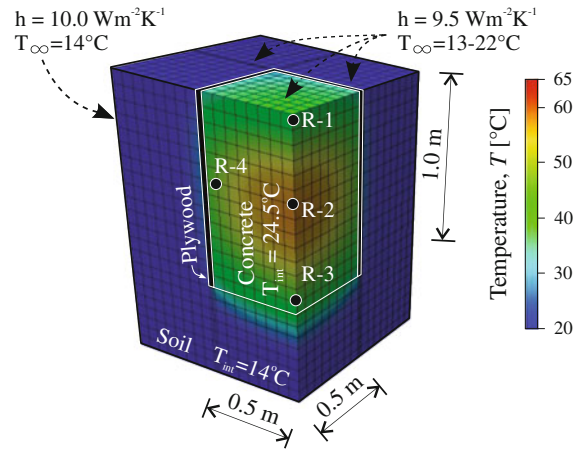
Fig. 4 Semi-adiabatic calorimeter: **a** calibration of the multi-scale model and **b** temperature field at 15.5 h

middle of the concrete cube. Table 2 specifies the used concrete mixture C1 as well as other further used mixtures. The properties of aggregates, which were determined in accordance with the guidelines defined in [5–8], are listed in Table 3.

The geometry was discretized into linear brick FEs and transferred into open-source OOFEM package [25]. Clinker of a binder (CP IV RS [4]) yielded potential hydration heat of 518.37 J/g; however, the used binder was a blended type with supplementary cementitious materials. It turned out from the simulations that 45 % of the binder needs to be replaced with any nonreactive material (e.g. fly ash + slag). The contribution of slag and fly ash is considered insignificant for the first days of hydration [27]. The effective amount of clinker is therefore $0.55 \times 420 = 230$ kg/m³ of concrete. The same clinker replacement ratio 0.45 in CP IV RS was used in all simulations.

The initial temperature of concrete was set at 24.5 °C according to temperature measurement. The thermal conductivity of concrete was assumed constant at 1.8 W m⁻¹ K⁻¹ during all simulations. This value is quite common in structural concretes [15, 19], although thermal conductivity slightly decreases when concrete binds more capillary water into hydration products [12]. The heat capacity of concrete was set at 870 J kg⁻¹ K⁻¹ during all simulations, which is a reasonable assumption [10]. The boundary conditions of the polystyrene insulation are detailed in Fig. 4b.

Hydration kinetics of the binder was calibrated from the semi-adiabatic setup. The parameters according to Eqs. (7) and (8) were fitted to $B_1 = 0.0007$ s⁻¹, $B_2 = 6.0e-5$, $\eta = 6.1$, $DoH_\infty = 0.85$, and $E_a = 38.3$ kJ/mol. The calibration of the model is displayed in Fig. 4a, which indicates that the hydration kinetics was fitted quite reasonably. The maximum temperature in the middle of the cube reached 55.2 °C after 15.5 h of hydration. Figure 4b displays the corresponding temperature field for a quarter of the cube at the temperature maximum.

4 Validation on a 1 m³ concrete block

Once the hydration model is calibrated, upscaling to a 1 m³ concrete block is straightforward. Figure 5 shows geometry, discretization, boundary conditions, and temperature field at 15.5 h. Notice that only a fourth of
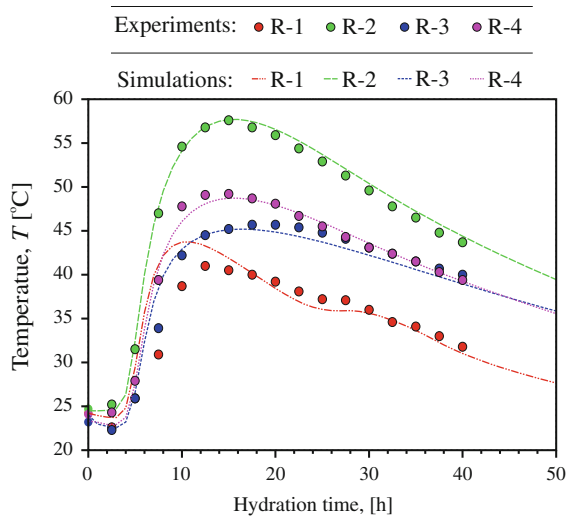
Fig. 6 Temperature evolution in temperature gauges on a 1 m³ concrete block

Table 4 Summary of thermal properties and boundary conditions on FB1 and FB2

Foundation block	FB1-511 m³	FB2-1,050 m³
Concrete mixture (Table 2)	C1	C3–C5
Concrete thermal conductivity (W m⁻¹ K⁻¹)	1.8	1.8
Concrete heat capacity (J kg⁻¹ K⁻¹)	870	870
Concrete density (kg/m³)	2,350	2,350
Number of concrete layers (–)	2	3
Initial temperature of each concrete layer (°C)	17.7	14.0
Heat capacity of the soil/rock (J kg⁻¹ K⁻¹)	840	840
Thermal conductivity of the soil/rock (W m⁻¹ K⁻¹)	0.80	0.80
Soil/rock density (kg/m³)	2,000	2,500
Initial temperature of the soil/rock (°C)	17.7	14.0

the block was modeled due to symmetry conditions. The same concrete mixture C1 was used, see Table 2.

The reference block was cast in a 30.0 mm thick open plywood formwork box buried in the ground. After casting, the block was covered with an impermeable plastic sheet and a 40.0 mm thick layer of water. Next, the whole system was covered with a 30.0 mm plywood formwork. The temperature in the reference block was monitored in four different points as depicted in Fig. 5.

Figure 6 validates the temperature evolution in the block. The results from the inner gauge R-1 deviate with the experimental measurements. This is likely because the gauge R-1 was placed on the surface of the concrete block and the measurements were therefore considerably affected by boundary conditions. Despite of that, the results from R-2,3,4 are good enough. The maximum temperature in gauge R-2 reached 55.5 °C at 15.5 h of hydration (Fig. 5).

5 Validation on 511 and 1,050 m³ foundation blocks

Temperature evolution in 511 m³ (FB1) and 1,050 m³ (FB2) foundation blocks presents a unique opportunity for validation. Both foundation blocks correspond to two high story residential buildings located in Santa Catarina, Brazil, having at least 35 floors.
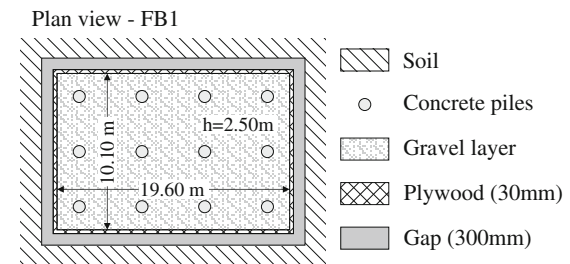

Fig. 7 Foundation block FB1-511 (m³)

The composition of all concrete mixtures used in the blocks are summarized in Table 2. The same binder CP IV RS is used with a known hydration kinetics from the 14 dm³ specimen (Sect. 3).

The thermal properties of concrete and corresponding boundary conditions of FB1 and FB2 are summarized in Table 4. In both models, the temperature at the top of the concrete block was kept constant. Additional information about each foundation block are presented along with the obtained results in the following subsections.

5.1 Foundation block FB1-511 m^3

The foundation block FB1-511 m^3 has the outer dimensions of 19.6 × 10.1 × 2.5 m. Details of the formwork, gravel bed, and dimensions of FB1 are illustrated in Fig. 7. Continuous casting of concrete was performed for about 12 h to prevent cold joints. Two concrete mixtures were used, namely C1 and C2, see Table 2.

C1 and C2 compositions differ slightly in the binder content and in the maximum dimension of the coarse aggregate, see Table 3. The use of a composition with aggregates of smaller dimension (C1) was due to the densely reinforced areas located at the bottom of the concrete block. The concrete mixture C2 was poured in the foundation block after the reinforcement at the bottom layer was completely covered with concrete.

After casting FB1, the exposed concrete surface of the block was covered with a layer of water to assure adequate curing of the mass concrete. This technique, known as ponding or flooding, permits to reduce the loss of moisture on concrete surface, thus preventing cracking at early-ages. Additionally, it helps reduce the heat transfer between the concrete and the ambient air, leading to a slower cooling process when combined with insulation systems [23]. The ACI Committee 207 [1] indicates that mass concrete is best cured with water in warm weather, which is our case.

The continuous casting was modeled as two concrete layers with time offset of 6 h. This led to a better temperature agreement in the upper layers of the block. Further simplification was made by using only C1 composition for the whole block. The details about geometry, mesh, boundary conditions, and temperature gauges in the foundation block FB1 are depicted in Fig. 8. Only one fourth of the block was modeled due to symmetry conditions.

The thermal properties of the soil at the bottom of FB1 as well as the initial temperature of soil and both concrete layers are summarized in Table 4. In total, 3840 brick FEs with 4,641 nodes created the
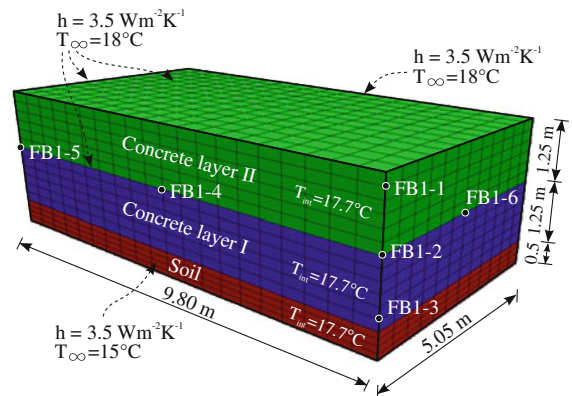

Fig. 8 FB1-511 m^3: geometry, mesh, boundary conditions, and temperature gauges

geometry. The integration time step was set to 2 h and 100 steps were executed. The computation ran for 10 min.

Figure 9a validates the temperature evolution in the block FB1. Inner gauges FB1-2,4,6 gave practically the same temperature evolution, which was only slightly influenced by the boundary conditions. The maximum temperature in gauges FB1-2,4,6 reached 65 °C at 74 h of hydration time. Figure 9b shows the corresponding temperature field and testifies that the soil temperature below the block increased.

5.2 Foundation block FB2-1,050 m^3

The second foundation block, namely FB2, is the main foundation block of a 42-floor building. The block has the dimensions of 20.1 × 20.1 × 2.6 m, which equals to 1,050 m^3 of concrete. Details of FB2 are shown in Fig. 10. Continuous casting could have been provided by the local ready-mixed concrete plant; nonetheless, the noise regulation of the town forbade this activity in the evening. For this reason, the concrete casting was divided in two working days, and retarder admixtures had to be added to offset hydration kinetics and thus avoid cold joints formation. The composition of the concrete mixtures used in FB2 is listed in Table 2.

The first layer of FB2, which is 1.60 m high, was being poured for approximately 11 h of the first working day. In particular, this layer was divided in two sub-layers. The first sub-layer is 1.40 m high and is composed of C3 concrete while the second one is 0.20 m high and is composed of C4. After that, a waiting period of 13 h was kept. During this period, the concrete remained fresh due to a high amount of
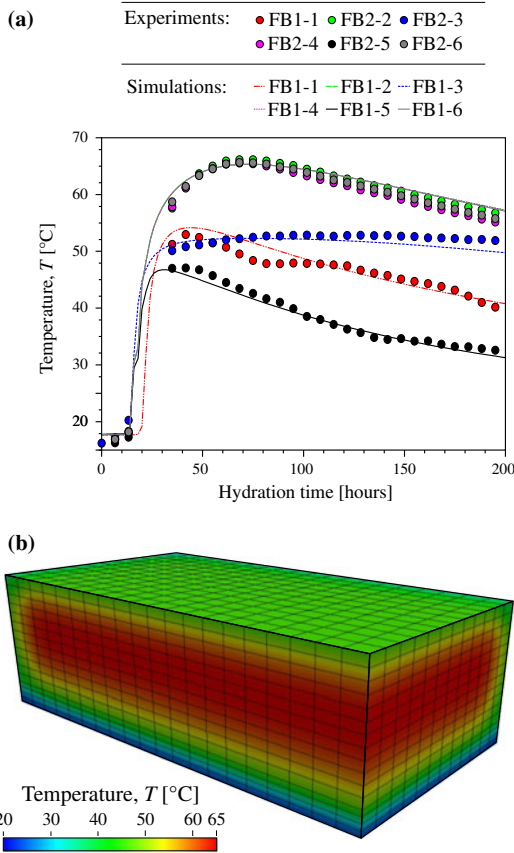
Fig. 9 Simulation results for FB1-511 m³: **a** temperature evolution and **b** temperature field at 74 h

Fig. 10 Foundation block FB2-1,050 m³

Fig. 11 Temperature curve of the mixtures C3–C5, and the corresponding retarding effect (+11 h for C3 and +32 h for C4)

retarder in C4. On the next working day, the concrete mixture C5 was poured for approximately 9 h to complete the second layer of the block, which is 1.00 m high. Curing by ponding or flooding was the same as with FB1.

The extended dormant period caused by the retarding admixture was quantified in a small semi-adiabatic calorimeter. Figure 11 shows the temperature curves for C3, C4, C5, and the corresponding retarding effect. The temperature curves highlight that all mixtures present similar hydration kinetics with various initial offsets; hence, the use of the same hydration kinetics after the offset is a reasonable assumption. Particularly, the retarding effect in C3 and C4 concrete was of 11 and 32 h, respectively.

Figure 12 provides details about geometry, mesh, boundary conditions, and temperature gauges in the foundation block FB2. Only one fourth of the block was modeled due to symmetry conditions. The thermal
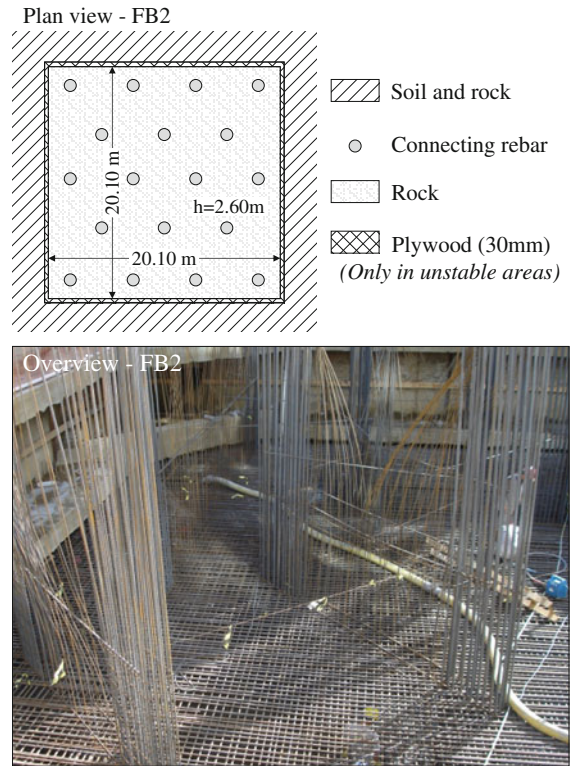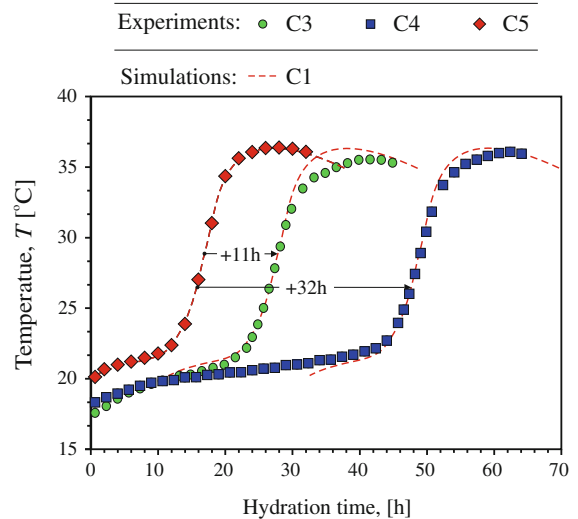
capacity of both the bedrock (bottom surface) and the soil (lateral surfaces) had to be taken into account. The values adopted in the simulations are listed in Table 4,
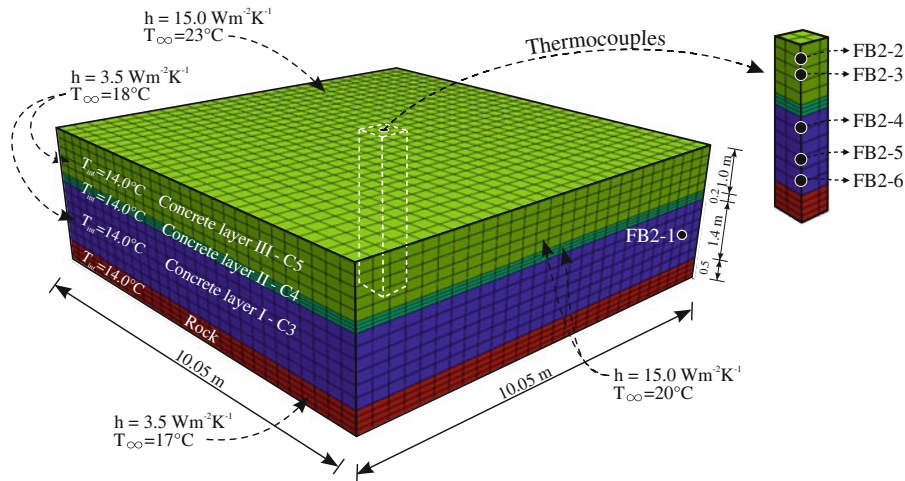
Fig. 12 FB2-1,050 m³: geometry, mesh, boundary conditions, and temperature gauges
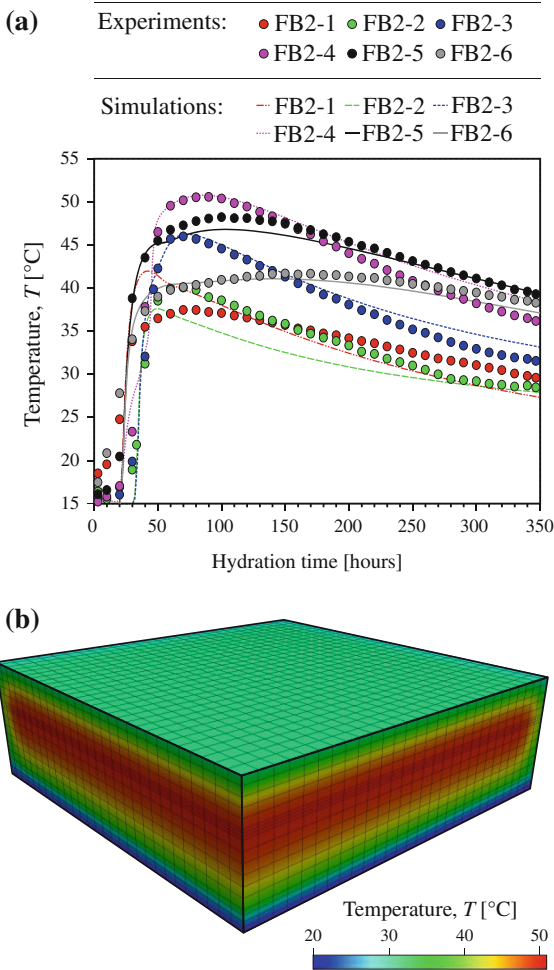

which also shows the initial temperature of soil, rock, and concrete layers.

Figure 13a validates the FB2 temperatures in all gauges. The gauges FB2-1 and FB2-2 show certain discrepancies. The most reasonable explanation is related to the misplacement of the gauges during concrete casting since the workers were not aware of it. The control of curing temperature could also present problems considering the large surface of the block. Because none of the possible sources of error can be proved, the results are presented as they were gathered.

The other gauges showed satisfactory agreement. This is likely because they were not affected considerably by the boundary conditions and possible misplacements would not be noticed in the measurements since the gauges are at the core of the concrete block. The maximum temperature in gauges FB2-3,4,5 reached 51 °C at 81 h of hydration. The corresponding temperature field is shown in Fig. 13b.

6 Conclusions

A unique set of experimental data proved that a calibrated affinity hydration model on a small-size concrete cube under semi-adiabatic conditions can be transferred to a mass concrete block with different boundary conditions on a much larger scale. The proposed semi-adiabatic procedure proved to be a suitable alternative to the standard isothermal calorimetry.

Fig. 13 Simulation results for FB2-1,050 m³: **a** temperature evolution and **b** temperature field at 81 h

Moreover, the models demonstrated that the combination of a proper mathematical formulation and a suitable affinity model for hydrating concrete is applicable to various shapes and sizes. The upscaling of small laboratory experiments to large-scale massive structures provides several advantages over traditional empirical methods, such as time-efficient simulation, virtual testing, and selection of suitable concrete mix. Ordinary Portland cements, blended cements, and various admixtures are covered automatically.

Calibrating the hydration model for ≈ 40 h enabled large-scale validation lasting for ≈ 350 h, which shows extrapolation by almost an order of magnitude. Upscaling of semi-adiabatic temperatures from small hydrating concrete specimens to large concrete volumes represents a highly attractive method for the concrete industry due to its low cost, high speed, and practicality.

References

1. ACI 207.1R-05: Guide to Mass Concrete (2005). Farmington Hills
2. Bamforth P (2003) Concreting large-volume (mass) pours. In Newman J, Choo BS (eds) Advanced concrete technology. Butterworth-Heinemann, Oxford, pp 1–47
3. Bentz D (2000) A three-dimensional cement hydration and microstructure development modeling package. Tech. Rep. Version 3.0. NIST Building and Fire Research Laboratory, Gaithersburg
4. Brazilian Association of Technical Standards: NBR 5736: Pozzolanic Portland Cement—Specification (1991). Rio de Janeiro, Brazil
5. Brazilian Association of Technical Standards: NBR 7219: aggregates for concrete—determination of pulverulent materials content—test method (2000). Rio de Janeiro, Brazil
6. Brazilian Association of Technical Standards: NBR NM248: aggregates—sieve analysis of fine and coarse aggregates (2003). Rio de Janeiro, Brazil
7. Brazilian Association of Technical Standards: NBR NM53: Coarse aggregate—determination of the bulk specific gravity, apparent specific gravity, and water absorption (2003). Rio de Janeiro, Brazil
8. Brazilian Association of Technical Standards: NBR 7212: aggregates for concrete—specification (2005). Rio de Janeiro, Brazil
9. Cervera M, Oliver J, Prato T (1999) Thermo-chemo–mechanical model for concrete. I: hydration and aging. J Eng Mech ASCE 125(9):1018–1027. doi:10.1061/(ASCE)0733-9399(1999)125:9(1018)
10. Choktaweekarn P, Tangtermsirikul S (2010) Effect of aggregate type, casting, thickness and curing condition on restrained strain of mass concrete. Songklanakarin J Sci Technol 32(4):391–402
11. Coussy O (1995) Mechanics of porous media. Wiley, New York
12. Faria R, Azenha M, Figueiras JA (2006) Modelling of concrete at early ages: application to an externally restrained slab. Cem Concr Compos 28(6):572–585. doi:10.1016/j.cemconcomp.2006.02.012
13. Gawin D, Pesavento F, Schrefler BA (2006) Hygro-thermo-chemo-mechanical modelling of concrete at early ages and beyond. part i: hydration and hygro-thermal phenomena. Int J Numer Methods Eng 67(3):299–331. doi:10.1002/nme.1615
14. Gawin D, Pesavento F, Schrefler BA (2006) Hygro-thermo-chemo-mechanical modelling of concrete at early ages and beyond. part ii: shrinkage and creep of concrete. Int J Numer Methods Eng 67(3):332–363. doi:10.1002/nme.1636
15. Guo L, Guo L, Zhong L, Zhu Y (2011) Thermal conductivity and heat transfer coefficient of concrete. J Wuhan Univ Technol Mater Sci Ed 26(4):791–796. doi:10.1007/s11595-011-0312-3
16. Hellmich C, Mang HA, Ulm FJ (2001) Hybrid method for quantification of stress states in shotcrete tunnel shells: combination of 3D in situ displacement measurements and thermochemoplastic material law. Comput Struct 79(22–25):2103–2115. doi:10.1016/S0045-7949(01)00057-8
17. Hughes TJR (2000) The Finite element method: linear static and dynamic finite element analysis. Dover Publications, Mineola
18. Jendele L, Šmilauer V, Červenka J (2013) Multiscale hydro-thermo-mechanical model for early-age and mature concrete structures. Adv Eng Softw. doi:10.1016/j.advengsoft.2013.05.002
19. Kim KH, Jeon SE, Kim JK, Yang S (2003) An experimental study on thermal conductivity of concrete. Cem Concr Res 33(3):363–371. doi:10.1016/S0008-8846(02)00965-1
20. Kosmatka S, Kerkhoff B, Panarese W (2003) Design and control of concrete mixtures, 14th edn. Portland Cement Association, Skokie
21. Mehta P, Monteiro P (2005) Concrete: microstructure, properties, and materials. McGraw-Hill, New York
22. Nawy E (2008) Concrete Construction engineering handbook, 2nd edn. CRC Press, Boca Raton
23. Neville AM (1997) Properties of concrete, 4th edn. Wiley, London
24. NRMCA (2007) Concrete in practice. National Ready Mixed Concrete Association, Silver Spring
25. Patzák B, Rypl D (2012) Object-oriented, parallel finite element framework with dynamic load balancing. Adv Eng Softw 47(1):35–50. doi:10.1016/j.advengsoft.2011.12.008
26. Ulm FJ, Coussy O (1998) Couplings in early-age concrete: from material modeling to structural design. Int J Solids Struct 35(31–32):4295–4311. doi:10.1016/S0020-7683(97)00317-X
27. Šmilauer V (2013) Multiscale hierarchical modeling of hydrating concrete. Saxe-Coburg Publications, Stirling

28. Štemberk P, Rainová A (2011) Simulation of hydration and cracking propagation with temperature effect based on fuzzy logic theory. Mechanika 17(4):358–362. doi:10.5755/j01.mech.17.4.561

29. Weiss W, Yang W, Shah S (1999) Factors influencing durability and early-age cracking in high strength concrete structures. In: High performance concrete: research to practice, SP 189-22. American Concrete Institute, Farmington Hills, pp 387–409